

**The chemical suitability for recycling of zinc contaminated steelmaking by-product dusts: The case of the UK steel plant**

STEWART, Daniel, SCRIMSHIRE, Alex, THOMSON, David, BINGHAM, Paul <<http://orcid.org/0000-0001-6017-0798>> and BARRON, Andrew

Available from Sheffield Hallam University Research Archive (SHURA) at:

<https://shura.shu.ac.uk/29877/>

---

This document is the Published Version [VoR]

**Citation:**

STEWART, Daniel, SCRIMSHIRE, Alex, THOMSON, David, BINGHAM, Paul and BARRON, Andrew (2022). The chemical suitability for recycling of zinc contaminated steelmaking by-product dusts: The case of the UK steel plant. *Resources, Conservation & Recycling Advances*, 14, p. 200073. [Article]

---

**Copyright and re-use policy**

See <http://shura.shu.ac.uk/information.html>



# The chemical suitability for recycling of zinc contaminated steelmaking by-product dusts: The case of the UK steel plant

Daniel J.C. Stewart<sup>a</sup>, Alex Scrimshire<sup>b</sup>, David Thomson<sup>c</sup>, Paul A. Bingham<sup>b</sup>, Andrew R. Barron<sup>a,d,e,f,\*</sup>

<sup>a</sup> Energy Safety Research Institute (ESRI), Swansea University, Bay Campus, Swansea, SA1 8EN, UK

<sup>b</sup> Materials and Engineering Research Institute, Sheffield Hallam University, Sheffield, S1 1WB, UK

<sup>c</sup> Tata Steel Strip Products UK, Port Talbot, SA13 2NG, UK

<sup>d</sup> Arizona Institute for Resilient Environments and Societies (ARIES), University of Arizona, Tucson, Arizona 85719, USA

<sup>e</sup> Department of Chemistry and Department of Materials Science and Nanoengineering, Rice University, Houston, Texas 77005, USA

<sup>f</sup> Faculty of Engineering, Universiti Teknologi Brunei, Brunei Darussalam

## ARTICLE INFO

### Keywords:

Basic oxygen steelmaking  
Blast furnace  
Dust  
Zinc removal  
Recycling  
Rotary hearth furnace  
Material characterization  
BF dust  
BOS Dust

## ABSTRACT

Basic oxygen steelmaking (BOS) dust and blast furnace (BF) dust from former and operating steelmaking facilities in the United Kingdom have been characterized by MP-AES, SEM-EDX, particle size analysis, TGA-DSC, combustion analysis, <sup>57</sup>Fe Mössbauer spectroscopy, and powder XRD. These materials are a potentially valuable source of Fe for ironmaking, but their contamination with zinc precludes their recycling via the conventional sinter plant/BF route. XRD suggested some of the zinc present in the material is in the form of sub-stoichiometric zinc ferrites  $Zn_xFe_{3-x}O_4$ , making hydrometallurgical separation less effective. BF dust contains 40 wt.% levels of fixed carbon ( $C_{fix}$ ) indicating it could be useful as an alternative reductant in rotary hearth furnace processes such as FASTMET. The rotary hearth furnace appears to be the most suited separation technique available due to its lack of sensitivity to zinc present in zinc ferrite compounds, and reintegration of the recovered iron into the steelmaking process.

## 1. Introduction

Steelmaking via the blast furnace/basic oxygen steelmaking process naturally generates ferrous bearing by-product dusts. These can be formed by abrasion during handling of bulk products, such as ore in the case of iron ore fines (Halt et al., 2015), abrasion during hot rolling or casting (Bagatini et al., 2011) or they are recovered from off-gas systems in the case of flue dusts (Nyridena, 1991). Typically, these fine materials sometimes known as 'revert' materials are recycled through integration into the sintering process. This process agglomerates the fine material into a strong lumpy product known as sinter, which is then suitable for charging to the BF where it is then smelted alongside virgin material and the iron content is recovered.

Two key fine materials that are a consistent challenge to recycle are BOS Dust and BF dust, sometimes referred to as slurry or filtercake (Stewart and Barron, 2020). These materials are scrubbed from the off-gas systems of the basic oxygen furnace (BOF) and blast furnace (BF) respectively and the barrier to their reintegration into the ironmaking

process is their contamination with zinc. High zinc loading has a well-studied detrimental effect of BF performance (Besta et al., 2013; Klut et al., 2016; Onoye et al., 1981) and as such, zinc content is tightly controlled to levels around 120–200 g/tHM (tHM = Tonnes of Hot Metal) for most industrial furnace operations. Zinc removal processes for these materials have been thoroughly studied and commercialized over the past 50 years and reviewed recently (Stewart and Barron, 2020) and the rotary hearth furnace (RHF) is the key emerging technology for removal of zinc from these by-products.

RHF processes such as FASTMET (McClelland and Metius, 2003), DRYIron (Ichikawa and Morishige, 2002), and INMETCO (Hanewald et al., 1992) utilize self-reducing agglomerates fired in a rotating turntable furnace to temperatures around 1300 °C for 12 - 22 min. Zinc is reduced by carbon present in the briquettes and vaporized; the zinc vapor reoxidizes in the hot off-gas and is collected as a crude oxide from the off-gas system of the furnace. The key advantages of the RHF are that the iron product discharged from the furnace is highly metallized (>80%) and mechanically strong enough to be charged to a BF. This

\* Corresponding author.

E-mail address: [a.r.barron@swansea.ac.uk](mailto:a.r.barron@swansea.ac.uk) (A.R. Barron).

<https://doi.org/10.1016/j.rcradv.2022.200073>

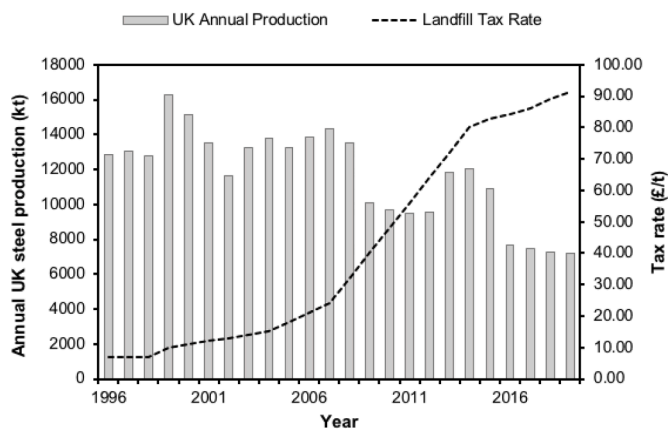


**Fig. 1.** UK crude steel annual production output (kt) and UK landfill tax rates (£/t). Data adapted from World Steel Association annual production statistics (World Steel Association, 2018) and the UK government respectively (HM Revenue and Customs, 2020).

high degree of pre-reduction can decrease fuel rates within the BF leading to higher throughput and reducing requirements for expensive and environmentally costly coking coals. A case study at Tata Steel India reported a 6% coke rate reduction with the addition of 100–150 kg/tHM 5–18 mm DRI to the BF (Chatterjee, 2012). Another key advantage of the RHF is the tremendous flexibility in reducing agent selection in the self-reducing briquettes, alternative reductants including steaming coal (Holappa and Kekkonen, 2000), waste plastic (Dankwah et al., 2015), biomass (Yuan et al., 2017), and BF dust (Mombelli et al., 2016).

Developments in the field have meant that a solid waste processing solution such as RHF are becoming more commercially attractive but much of this potentially valuable zinc and iron resource has been landfilled or stockpiled, creating an environmental liability but also a commercial opportunity. This is especially true in westernized economies such as the United Kingdom. Landfill tax rates have increased dramatically in the UK since their inception in 1996 as the government has sought to reduce the environmental impact of industrial activity (Fig. 1). The decline of the UK steelmaking industry (Fig. 1) has also led to large deposits of iron-bearing material left at sites no longer operating as full integrated plants, or no longer operating altogether.

No accurate estimates of the total scale of waste iron oxide stockpiles in the UK exist as of the time of writing, but Mackillop estimates substantial ferrous resource in the form of ad-hoc stockpiles (MacKillop, 2009) Fig. 2. shows key ironmaking sites within the UK. Remediation of land used for ironmaking is an area of key concern for the UK government. Following the closure of the Ravenscraig British Steel plant in Scotland, there was a great deal of controversy surrounding the remediation of the land that the steel plant occupied: an estimated 284,000 m<sup>3</sup> (355,000 – 542,000 tonnes) of stockpiled filtercake dust was left at the site following the termination of production (ENDS Report, 1992).

To recover legacy material from now defunct ironmaking sites, as well as recover iron and zinc units from by-product dusts and sludges as they are produced to prevent formation of stockpiles, a commercially viable recovery process is required. The first step in a viable recycling solution of these materials is characterization of them to determine their suitability for recovery through established processes such as the RHF.

There are several pertinent questions about the chemical composition of the dusts that need to be examined in detail to determine their suitability for recycling:

- What form is the zinc in the dust present in?
- Do the dusts contain any hazardous heavy metal elements that may preclude their safe handling and processing?
- How much of the iron present within the samples is in the metallic form?

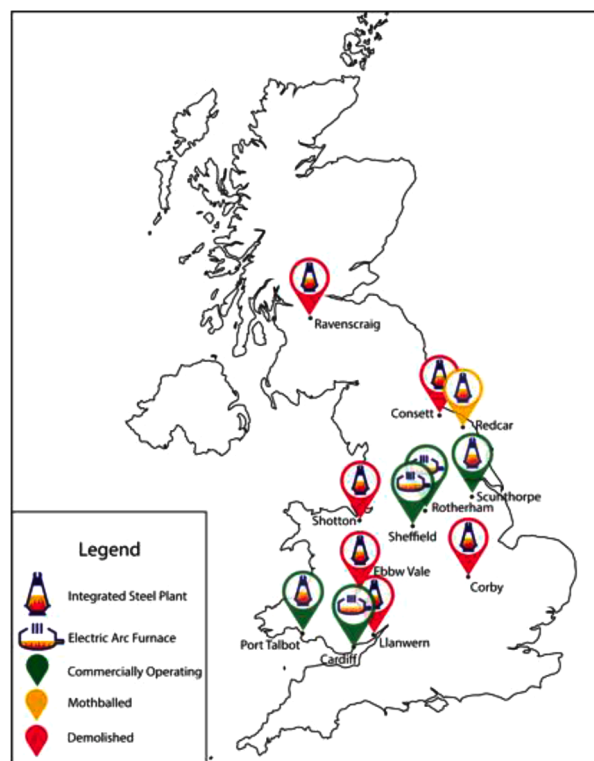


**Fig. 2.** Major steelmaking production facilities in the UK since 1980. ‘Heavy end’ iron production closures occurred as follows: Ebbw Vale (1978), Corby, Shotton, Consett (1980), Ravenscraig (1992), Llanwern (2001), (British Steel, n. d.; Rhodes, 2018) Map adapted with permission (d-maps, 2020).

Much of the established literature characterizing BOS dust material typically focuses on non-stockpiled materials at a single production location (Stewart and Barron, 2020). A thorough analysis of stockpiled material from three major production facilities in close geographic proximity such as in this article, would allow for greater insight into the scalability of any industrial scale recovery process. A large-scale zinc separation plant in the UK would likely process legacy material from a wide range of locations, and certain separation techniques such as hydrometallurgical recovery of zinc are significantly more sensitive to input material variability.

## 2. Methods

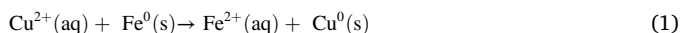
### 2.1. Materials and chemicals

Samples of BOS dust and BF dust were taken from a single integrated works in the UK, and are referred to as BOS Dust A and BF Dust A. Samples of BOS dust was also obtained from a further two integrated plants in the UK, those samples will be referred to as BOS Dust B and BOS Dust C. Samples (10 kg) of each material were dried at 90 °C and deagglomerated until the material passed 500 µm for analysis. All reagents used in chemical analysis were of ACS grade.

### 2.2. Analytical techniques

For trace metal analysis, samples were digested at 120 °C for 90 min using a DigiPREP Jr. graphite heating block digestion system in HNO<sub>3</sub> (9 cm<sup>3</sup>, 69%) and HCl (3 cm<sup>3</sup>, 37%). Once cooled, H<sub>2</sub>O<sub>2</sub> (3 cm<sup>3</sup>, 50%) was added dropwise to oxidize any residual carbonaceous matter. Samples were then filtered through a 0.45 µm filter. The samples were then diluted and analyzed via an Agilent 4210 MP-AES for trace metal contents against a reagent blank. Determination of metallic iron content (% Fe<sub>met</sub>) was performed using an adapted methodology (Xu et al., 2003)

within a DigiPREP Jr. Graphite heating block. The analyte was reacted for 90 min at 120 °C in CuSO<sub>4</sub> solution (20 cm<sup>3</sup>, 1 mol/dm<sup>3</sup>) maintaining the solution at pH 7.0. The reaction vessel was then hot filtered and acidified to pH 1.0 using HCl (1 cm<sup>3</sup>, 37%) and diluted and analyzed via an Agilent 4210 MP-AES for Fe determination against a reagent blank. The aqueous Cu<sup>2+</sup> ion selectively oxidizes any metallic iron present in the powdered sample via:



Analysis of the resultant solution for Fe by MP-AES directly relates to the amount of metallic Fe in the sample. The ratio of iron present in the metallic state (%Metallization) was determined in comparison with the total iron content (as determined by XRF):

$$\% \text{Metallization} = \frac{\text{Fe}_{\text{metal}}}{\text{Fe}_{\text{total}}} \times 100 \quad (2)$$

Quantitative X-Ray fluorescence analysis was performed by the Basic Oxygen Steelmaking Laboratory team at Tata Steel Port Talbot. Detected elements (Si, Ca, Mg, Fe, Ti, P, Al and Mn) were balanced with oxygen to allow for basicity calculations apart from iron due to it routinely existing in multiple oxidation states within ironmaking materials. Basicity was calculated using the following equations (Meraikib, 1995):

$$B_1 = \frac{\text{CaO}}{\text{SiO}_2} \quad (3)$$

$$B_2 = \frac{\text{CaO} + \text{MgO}}{\text{SiO}_2 + \text{P}_2\text{O}_5} \quad (4)$$

$$B_3 = \frac{\text{CaO} + \text{MgO}}{\text{SiO}_2 + \text{Al}_2\text{O}_3} \quad (5)$$

$$B_4 = \frac{\text{CaO} + \text{MgO}}{\text{SiO}_2 + \text{Al}_2\text{O}_3 + \text{P}_2\text{O}_5} \quad (6)$$

$$B_5 = \frac{\text{CaO} + \text{MgO} + \text{MnO}}{\text{SiO}_2 + \text{Al}_2\text{O}_3 + \text{P}_2\text{O}_5} \quad (7)$$

Carbon and sulfur content were quantitatively determined using an Eltra CS500 combustion analyzer. Powder X-ray Diffraction analysis was performed using a Panalytical Empyrean S3 (Co-K<sub>α</sub> λ = 1.7902 Å, 10 – 120°, s = 0.066°, t = 20 s). A Hitachi tabletop TM3030 Scanning Electron Microscope was used to provide morphological information. Thermogravimetric information was obtained using an Q600 SDT model TGA-DSC using an alumina crucible, heating rate of 5 °C/min and a flow rate of 100 cm<sup>3</sup>/min of either carbon dioxide, argon or compressed air dependent on the experimental protocol. Particle size analysis was undertaken using a Malvern Panalytical Mastersizer 3000 with samples mechanically dispersed in isopropanol.

For transmission <sup>57</sup>Fe Mössbauer spectroscopy measurements, acrylic absorber discs with a sample area of 1.767 cm<sup>2</sup> were with each sample. The 14.4 keV γ-rays were supplied by the cascade decay of 25 mCi <sup>57</sup>Co in Rh matrix source, oscillated at constant acceleration by a SeeCo W304 drive unit, and detected using a SeeCo 45,431 Kr proportional counter operating with 1.785 kV bias voltage applied to the cathode. All measurements were carried out over a velocity range of ±12 mm/s due to the presence of high-field magnetic splitting and were calibrated relative to α-Fe foil. Spectral data were fitted using the Recoil software package (Rancourt, 1998), using Lorentzian line shapes.

### 3. Results and discussion

#### 3.1. Microwave plasma – atomic emission spectroscopy

##### 3.1.1. Trace metals analysis

Trace metals analysis of the materials indicated sizeable contamination with zinc (Table 1). Levels of toxic heavy metals such as cadmium

**Table 1**  
Trace metal analysis results for BOS Dust A, BF Dust A, BOS Dust B, and BOS Dust C material.

Material	Composition (wt.%)															
	As	B	Ba	Cd	Co	Cr	Cu	K	Mo	Na	Ni	Pb	Sb	V	Zn	Total
BOS Dust A	<0.005	<0.005	0.020	<0.005	<0.005	0.016	<0.005	0.015	<0.005	0.065	0.006	0.15	<0.005	0.027	2.74	3.04
BF Dust A	<0.005	<0.005	<0.005	<0.005	<0.005	<0.005	<0.005	0.140	<0.005	0.046	<0.005	0.18	<0.005	0.013	0.89	1.27
BOS Dust B	<0.005	<0.005	<0.005	<0.005	<0.005	<0.005	0.01	0.114	<0.005	0.16	<0.005	0.08	<0.005	0.017	0.41	0.79
BOS Dust C	<0.005	<0.005	<0.005	<0.005	<0.005	<0.005	0.01	0.065	<0.005	0.10	<0.005	0.22	<0.005	<0.005	1.70	2.10

**Table 2**

Metallic iron analysis for BOS Dust A, BF Dust A, BOS Dust B and BOS Dust C material.

Material	Fe <sub>Met</sub> (wt.%)	%Metallization
BOS Dust A	14.20	23.63
BF Dust A	0.76	2.84
BOS Dust B	13.50	22.56
BOS Dust C	0.60	1.12

and arsenic were found to be below the detectable limit of the analyses. The Zn levels would be too high to recycle any of the dusts at scale via a sinter plant/blow furnace without some form of pre-treatment process to reduce zinc content, typical limitations for zinc loading to a BF is 100–200 g/tHM (Stewart and Barron, 2020). Small amounts of lead were detected in the samples, which appears consistent with results from other studies on similar materials (Cantarino et al., 2012; Trung et al., 2011).

### 3.1.2. Metallic iron analysis

Analysis for metallic iron (Table 2) showed that as expected the BOS dust materials contain substantial metallic iron.

BOS Dust C was anomalous to BOS Dust A and BOS Dust B however, in that it was significantly less metallized in terms of iron. There are a few plausible explanations for this; firstly, storage conditions of by-product dusts can have a dramatic effect on material chemistry (Jaafar, 2014). The process conditions during the blow in the BOS vessel can have a significant effect on the morphology of the dusts (Steer et al., 2014). Finally, the stockpiles that these materials are stored in are heterogenous and can contain many different types of materials; it is possible that BOS Dust C contains non-BOS dust material as well.

The substantial metallization of the BOS Dust A and BOS Dust B samples make them especially strong candidates for pyrometallurgical recovery, due to the associated reduction in carbon requirement.

### 3.2. X-Ray fluorescence (XRF) spectroscopy

The results of the XRF analysis indicated some stark differences in the chemical composition of the materials (Table 3). In particular, it is worth noting that the iron content was highly variable. This is to be expected as the degree of oxidation of the material from its initial condition will depend on variables such as storage conditions and age of the material which is difficult to know for certain. The BOS dust materials all contained a substantial amount of Ca and Mg, and they are all predominately basic in nature, with oxide basicity greater than 1 as shown in Table 4. This is likely owing to the basic nature of the BOS process in which they were produced (Ray et al., 1997). BF Dust A is a clear outlier; it has substantially lower Fe content than the other materials and is much more acidic in terms of the mineral oxides that are present. This is due to the acidic nature of the iron ore used in the blast furnace (Salama et al., 2015) which is likely the source of the iron within the dust.

### 3.3. Powder X-ray diffraction (XRD)

The powder XRD patterns of the four materials show distinct differences in morphology that are not clear through chemical analysis alone (Fig. 3). All three BOS dust samples were found to contain

**Table 3**

XRF analysis results for BOS Dust A, BF Dust A, BOS Dust B, and BOS Dust C material.

Material	Fe <sub>Tot</sub>	SiO <sub>2</sub>	Al <sub>2</sub> O <sub>3</sub>	TiO <sub>2</sub>	CaO	MgO	P <sub>2</sub> O <sub>5</sub>	MnO	Total
BOS Dust A	60.09	2.31	0.34	0.06	10.67	1.16	0.088	0.74	75.46
BF Dust A	26.79	5.61	2.63	0.14	3.86	0.77	0.159	0.19	40.15
BOS Dust B	59.83	2.98	0.65	0.08	6.66	1.91	0.133	1.48	73.72
BOS Dust C	53.73	2.71	0.70	0.07	4.71	1.14	0.159	1.16	63.22

substantial metallic iron, which is corroborated with the MP-AES analysis results for selective metallic iron in Section 2.1.2.

As expected, the BOS dust samples all appear to be significantly reduced. Metallic iron was detected in all three. The XRD diffraction patterns suggest that BOS Dust A contains iron predominantly in the Fe<sup>0</sup> or Fe<sup>2+</sup> oxide form, with small amounts of mixed Fe<sup>2+</sup>/Fe<sup>3+</sup> and Fe<sup>3+</sup> oxide. BOS Dust B and BOS Dust C show a varied mix of iron phases, with comparatively a smaller proportion of Fe<sup>0</sup> and Fe<sup>2+</sup> oxide relative to the higher iron oxides.

BF Dust A shows a broad peak (2θ = 28° - 31°), consistent with the presence of amorphous carbon (Manoj, 2016), which is typical of coal and coke bearing materials. In contrast, both BOS Dust C and BOS Dust B appear to contain intense sharp peaks (2θ = 31°) consistent with graphitic material (Manoj, 2016) this may be 'kish' graphite, which can be formed from the cooling of carbon saturated liquid iron (Liu and Loper, 1991).

All four samples appeared to show a diffraction pattern similar to the magnetite spinel; however, due to the zinc content of the materials it is possible that some of the tetrahedral sites within the spinel are occupied by Zn<sup>2+</sup> rather than Fe<sup>2+</sup> as in franklinite (ZnFe<sub>2</sub>O<sub>4</sub>). Large quantities of zinc being present in the spinel phase rather than as ZnO has negative implications for hydrometallurgical recovery (Stewart and Barron, 2020).

Al-Anazi et al. compared the effect of increasing Zn occupation of tetrahedral sites in the magnetite spinel on the (311) plane (using powder X-ray diffraction) and noted that increasing occupancy of those sites with Zn corresponded with an increase in the lattice parameter of the unit cell of crystal lattice (Al-Anazi et al., 2020). Calculation of the lattice parameter (*a*) of the cubic spinel phase of each material is shown in Table 5. Crystal lattice parameters for the materials were determined by examination of the position of the spinel peaks on the diffraction patterns at ~21.3° and ~35.1° due to their lack of overlap with peaks related to other crystalline phases in the materials.

BOS Dust A showed a cell parameter slightly smaller than anticipated for pure magnetite (*a* = 8.3708 Å). This result may suggest the spinel phase is slightly deficient in tetrahedral Fe<sup>2+</sup> occupancy, more similar to a maghemite structure (Ruíz-Baltazar et al., 2015), and also suggests that the spinel phase in the material does not contain Zn<sup>2+</sup> in tetrahedral occupancy. BF Dust A (8.3972 Å) was determined to have a cell parameter extremely consistent with pure magnetite (8.394 Å) (Zhang and Xu, 2020).

BOS Dust B and BOS Dust C show a slightly elevated lattice constant more consistent with sub-stoichiometric ZnFe<sub>2</sub>O<sub>4</sub>. Specifically, the lattice constant corresponds well with literature examples for Zn<sub>0.189</sub>Fe<sub>2.811</sub>O<sub>4</sub> (Å = 8.403) (Yang et al., 2013) and Zn<sub>0.35</sub>Fe<sub>2.65</sub>O<sub>4</sub> (Å = 8.408) (Kmita et al., 2021). While this analysis is only qualitative, the levels of zinc removal required for economic recovery of these materials

**Table 4**

Calculated basicity for material from BOS Dust A, BF Dust A, BOS Dust B, and BOS Dust C.

Material	B <sub>1</sub>	B <sub>2</sub>	B <sub>3</sub>	B <sub>4</sub>	B <sub>5</sub>
BOS Dust A	4.62	4.93	4.46	4.32	4.59
BF Dust A	0.69	0.80	0.56	0.55	0.57
BOS Dust B	2.23	2.75	2.36	2.28	2.67
BOS Dust C	1.74	2.04	1.72	1.64	1.96

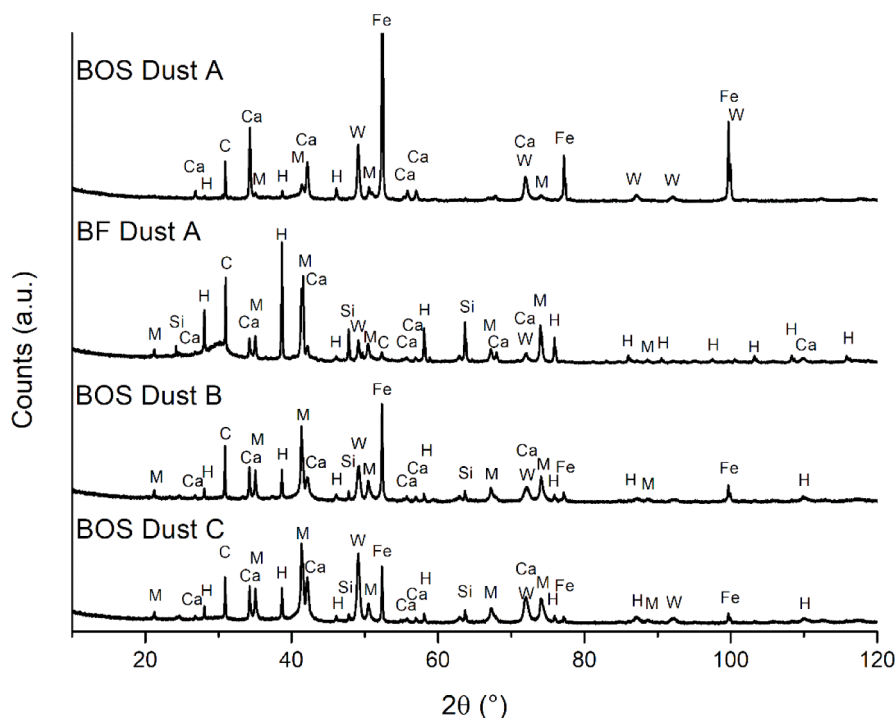


**Fig. 3.** Powder XRD patterns for BOS Dust A, BF Dust A, BOS Dust B and BOS Dust C. Ca = Calcite ( $\text{CaCO}_3$  - COD# 1,010,962), H = hematite ( $\text{Fe}_2\text{O}_3$  - COD# 9,009,782), C = graphite (C - COD# 9,011,577), M = Magnetite ( $\text{Fe}_3\text{O}_4$  - COD# 9,006,920), W = Wüstite ( $\text{FeO}$  - COD# 1,011,167), Fe =  $\alpha$ -iron (Fe - COD# 9,006,595), Si = quartz ( $\text{SiO}_2$  - COD# 500,035).

for recycling through the BF/BOS route is very high (~99%) and zinc occupation of tetrahedral sites within the spinel phase of the materials bodes poorly for effective and economical hydrometallurgical processing.

### 3.4. Thermogravimetric analysis and differential scanning calorimetry (TGA-DSC)

The TGA-DSC analysis of the four samples under an argon atmosphere is shown in Fig. 4. BOS Dust A shown three distinct transitions (Fig. 4a), a gradual endothermic mass loss between 0 and 200 °C of 2% which likely corresponds to the evaporation of moisture in the sample, an endothermic mass loss around 700 °C which appears consistent with the thermal decomposition of calcite (Souza and Braganc, 2013):



The third transition from 800 °C to 1000 °C of 4% is a little less clear, due to its exothermic nature it is not likely to be pyrolysis of volatile carbon species from the material. We propose that mass loss is likely to be the volatilization of zinc from the material (Bpt = 907 °C) (Zhang et al., 2020) with metallic iron acting as the reducing agent:



The zinc reduction reaction has been studied in detail with respect to the EAF dust with metallic iron added as the reducing agent for zinc

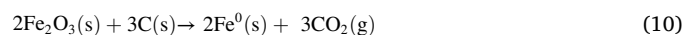
**Table 5**

Calculated lattice parameters for the spinel phase in each steel by-product dust sample.

Sample	(202)		(111)		Cell parameter(a, Å)
	2θ (°)	d (Å)	2θ (°)	d (Å)	
BOS Dust A	35.08	2.9704	21.30	4.8447	8.3708
BF Dust A	35.12	2.9670	21.29	4.8461	8.3972
BOS Dust B	35.11	2.9677	21.28	4.8478	8.4021
BOS Dust C	35.12	2.9645	21.28	4.8443	8.4020

oxide. (J J. Donald and Pickles, 1996.; Pickles, 2008). From the standard free energy change for this reaction ( $\Delta G^0 = 0$  at 1202 °C), it would be expected to only proceed to the right as that temperature is exceeded; however, it was found that the low partial pressure of zinc vapor caused by the presence of a sweeping gas flow, combined with the reaction promoting effects of CaO mean this reaction is feasible, albeit slow at temperatures as low as 800 °C and Zn(g) partial pressures around 0.001atm (J J. Donald and Pickles, 1996.). The observation that this reaction was occurring in the BOS Dust A was supported by the fact that the metallothermic reduction of zinc oxide by metallic iron is exothermic, which is in agreement with the DSC for the material (Fig. 4a) and by powder XRD of the sample (Fig. 5), which shows the phase changes after heating to 1000 °C. Metallic iron oxidized substantially to iron(II) oxide, which would not usually be expected under anoxic conditions. The presence of brownmillerite [ $\text{Ca}_2(\text{Al},\text{Fe})_2\text{O}_5$ ] is due to the reaction of CaO formed by the decomposition of calcite at 700 °C, reacting with Fe and Al oxides.

BF Dust A behaved in stark contrast to BOS Dust A under inert conditions however (Fig. 4b), the gradual mass decline from 0 - 600 °C is likely a combination of desorption of water from the material and pyrolysis of organic matter in the material. A slight endothermic mass loss at 700 °C is again characteristic of calcite decomposition. The mass loss from 900 - 1000 °C is not likely to be the metallothermic reduction of zinc oxide as reported for BOS Dust A due to the lack of metallic Fe available in the sample (Table 2) and the peaks endothermic character. This is instead likely to be carbothermal direct reduction of iron oxides in the material (Mikhail and Turcotte, 1998):



BOS Dust B (Fig. 4c) behaved quite similarly to BOS Dust A under inert atmosphere, with decomposition of calcite observed at 700 °C corresponding to a mass loss of 2.5%. The behavior between 800 °C and 1000 °C is different to PT BOS dust however, the mass loss is too large to simply be the loss of Zn and is endothermic in nature. It is likely that some carbothermal reduction is taking place between the solid fixed

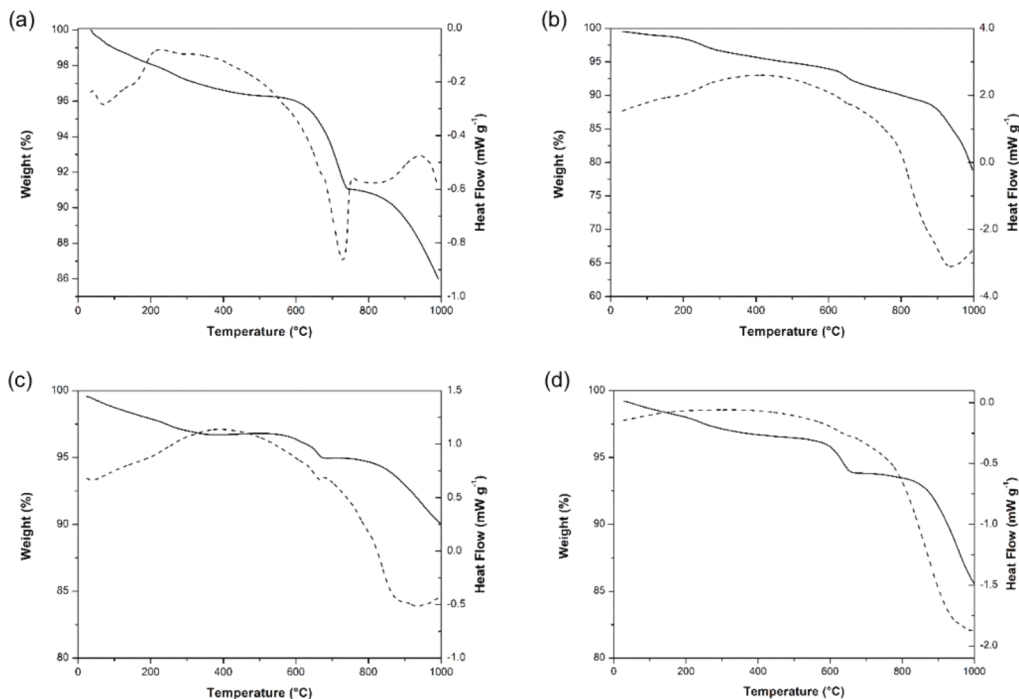


Fig. 4. TGA (solid line) and DSC (dashed line) results for (a) BOS Dust A, (b) BF Dust A, (c) BOS Dust B, and (d) BOS Dust C under an inert gas atmosphere.

carbon in the sample and the iron oxides as in the case of BF Dust A (Eqn (1)–(10)).

BOS Dust C behaved quite similarly to the sample from BOS Dust B, but the mass loss between 800 – 1000 °C attributed to carbothermal reduction of iron oxides is much more substantial (12% for BOS Dust C BOS versus 5% for BOS Dust B BOS), this is supported by the observation that BOS Dust C had a higher carbon content (Table 7) therefore more carbon available for reduction and thus, a greater mass loss during thermogravimetric analysis.

Fig. 6a shows that there are three discrete transitions as the BOS Dust

A is heated in air. Between 0 and 200 °C the mass loss is likely attributable to moisture loss, and a large exothermic mass gain of 10% at 400 °C corresponds well with the oxidation of metallic iron and lower iron oxides to Fe<sub>2</sub>O<sub>3</sub> (Lysenko et al., 2014). The second transition, at 700 °C, is the endothermic decomposition of calcite, like that observed under inert atmosphere. The sample continues to gain mass as T approached 1000 °C which is likely to be also attributable to oxidation of iron.

Fig. 6b shows the behavior of BF Dust A oxidized in air shows two clear exothermic transitions at 400 °C and 710 °C. The exothermic

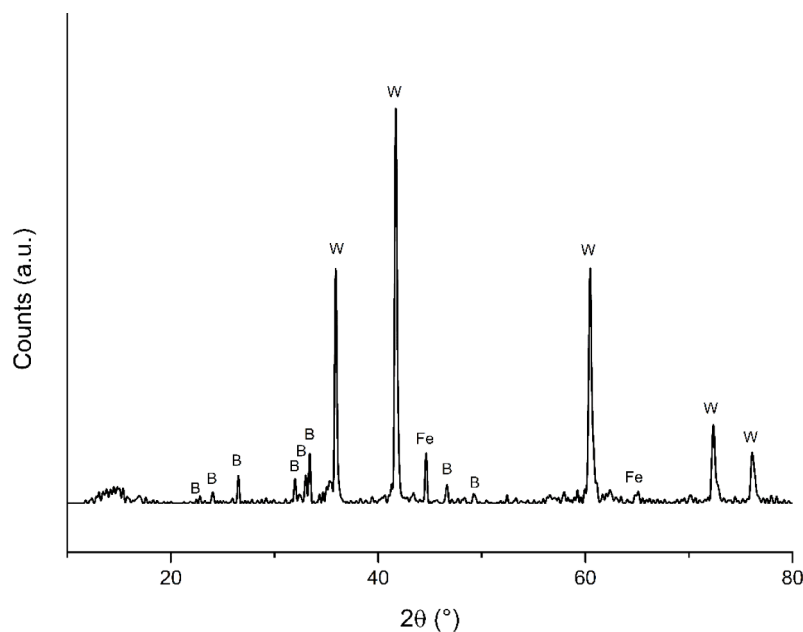


Fig. 5. Powder XRD pattern of BOS Dust A following TGA-DSC analysis at 1000 °C under an inert atmosphere. B = Brownmillerite (Ca<sub>2</sub>(Al, Fe)<sub>2</sub>O<sub>5</sub> – COD#9,014,319), W = Wuestite (FeO – COD# 1,011,167), Fe = α-iron (Fe – COD# 9,006,595).

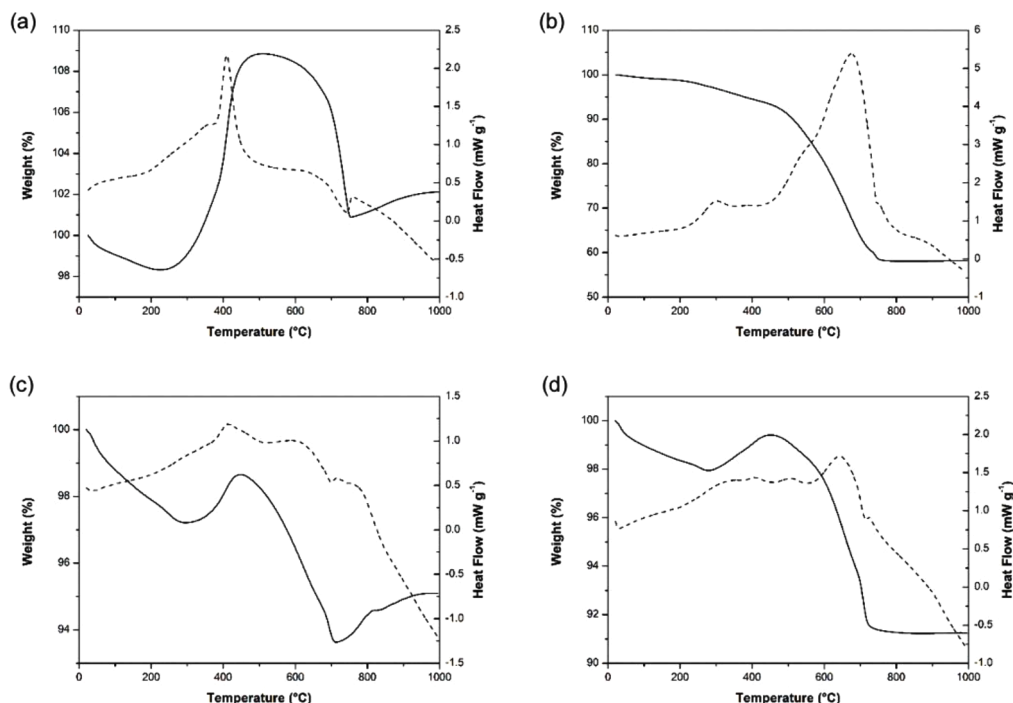


Fig. 6. TGA-DSC results for BOS Dust A (a), BF Dust A (b), BOS Dust B (c), and BOS Dust C (d) under a flow of compressed air. The DSC signals shown are exo-up.

transition at 400 °C is likely to be combustion of volatile organic matter, while the much larger exothermic transition at 710 °C is combustion of fixed carbonaceous matter. The decomposition of calcite seen in the material under an inert atmosphere is likely also present in Fig. 6b but is masked by the much larger combustion mass loss.

The TGA-DSC analysis for BOS Dust B and BOS Dust C (Fig. 6c and 6d) are quite similar. An initial mass loss between 0 and 200 °C is likely to be volatilization of water or breakdown of hydroxide materials. This transition is followed by an exothermic oxidation of iron at around 400 °C. A broad exothermic mass loss occurs for both samples between 450 °C and 700 °C which is likely to be combustion of organic and carbonaceous matter in the materials. Again, it is also likely that within

this region of the data endothermic carbonate decomposition, as can be seen by a small endothermic signal on the DSC for both samples at 700 °C.

BOS Dust B continued to increase in mass between 700 °C and 1000 °C which is likely to be further oxidation of iron. This is not observed in the BOS Dust C sample, which agrees with metallic iron analysis of the materials showing very low levels of metallic Fe in the material from BOS Dust C.

### 3.4. Particle size analysis

Laser diffraction particle size distributions of the four materials are

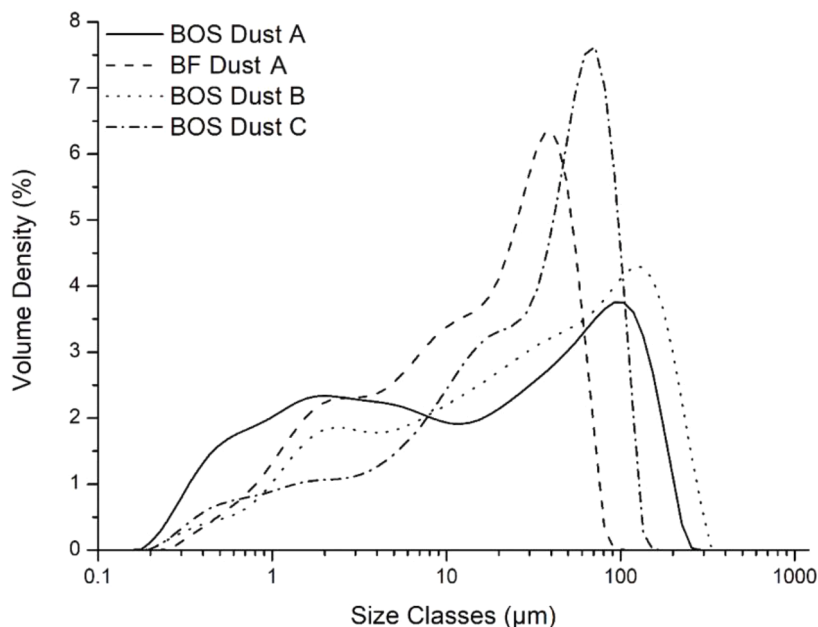


Fig. 7. Particle size distribution information for BOS Dust A, BF Dust A, BOS Dust B and BOS Dust C.

**Table 6**

Particle sizing data for BOS Dust A, BF Dust A, BOS Dust B and BOS Dust C.

Sample	D10 ( $\mu\text{m}$ )	D50 ( $\mu\text{m}$ )	D90 ( $\mu\text{m}$ )
BOS Dust A	0.75	12.54	118.2
BF Dust A	1.465	11.70	37.9
BOS Dust B	1.742	30.08	161.04
BOS Dust C	1.724	34.33	135.07

shown in Fig. 7 with D10, D50 and D90 particle diameter sizes shown in Table 6. It can be seen from the particle size analysis data that BF Dust A material is very fine, with 90% passing 37.9  $\mu\text{m}$ , an observation in reasonable agreement with analyses performed on similar material (Trinkel et al., 2016).

The BOS dust samples showed a particle size distribution broadly comparable to literature examples (Vereš et al., 2015). The BOS dust samples appeared to show two discrete particle types, extremely fine particles  $<5 \mu\text{m}$  and then a large number of particles close to the 100  $\mu\text{m}$  threshold. The slight differences in size distribution between BOS dust samples may be related to a number of factors, BOS vessel process parameters such as oxygen blowing velocity are known to have a direct effect on the material's physical properties, and the particle size distribution is known to change throughout the progress of a single blow (Steer et al., 2014).

Storage condition may also be a factor, some agglomeration of finer particles is to be expected. A study by Jaafar on material from Port Talbot showed that outdoor weathered BOS dust material from stockpiles had a substantially higher D90 value than fresh material even after grinding (Jaafar, 2014). The optimal particle size to produce high

compressive strength DRI from self-reducing briquettes as in a RHF is around 100  $\mu\text{m}$  (Narita et al., 2015) and a fine particle size is desirable for the purposes of accelerating the reduction and zinc removal reactions within the RHF as the reactions are surface area dependent (Kuwauchi, 2012).

### 3.5. Scanning electron microscopy

Scanning electron microscopy was utilized to observe the morphology of BF dust and BOS dusts from the three plants (Fig. 8). In the three BOS dusts (Fig. 8a, c and d) globular particles are clearly visible, and often coated with extremely fine particles. Larger agglomerations of ultrafine particles are also visible. In BF Dust A spheroidal particles are not observed, instead extremely fine angular particles are visible, including substantial amounts of carbon which appears as dark, flaky particles. Interestingly, in BOS Dust B and BOS Dust C these dark, flaky carbon particles can also be observed, but not in the BOS Dust A sample.

Cross sectional SEM analysis (Fig. 9) on each of the four materials show that the three BOS dust samples contain globular iron particles. These spheroids are formed by the ejection of droplets during the blowing period in a basic oxygen steelmaking vessel (Hahn and Neuschütz, 2002). Through the cross-sectional analysis of the materials, the metallic iron core of these spheroidal particles can be imaged. This result is in excellent agreement with the work of Kelebek (Kelebek et al., 2004) who first demonstrated this metallic iron core observation in BOS dust, and it can be seen in all three BOS dust samples in this study but not in the BF dust. The angular shape of the material in the BF Dust A suggests a

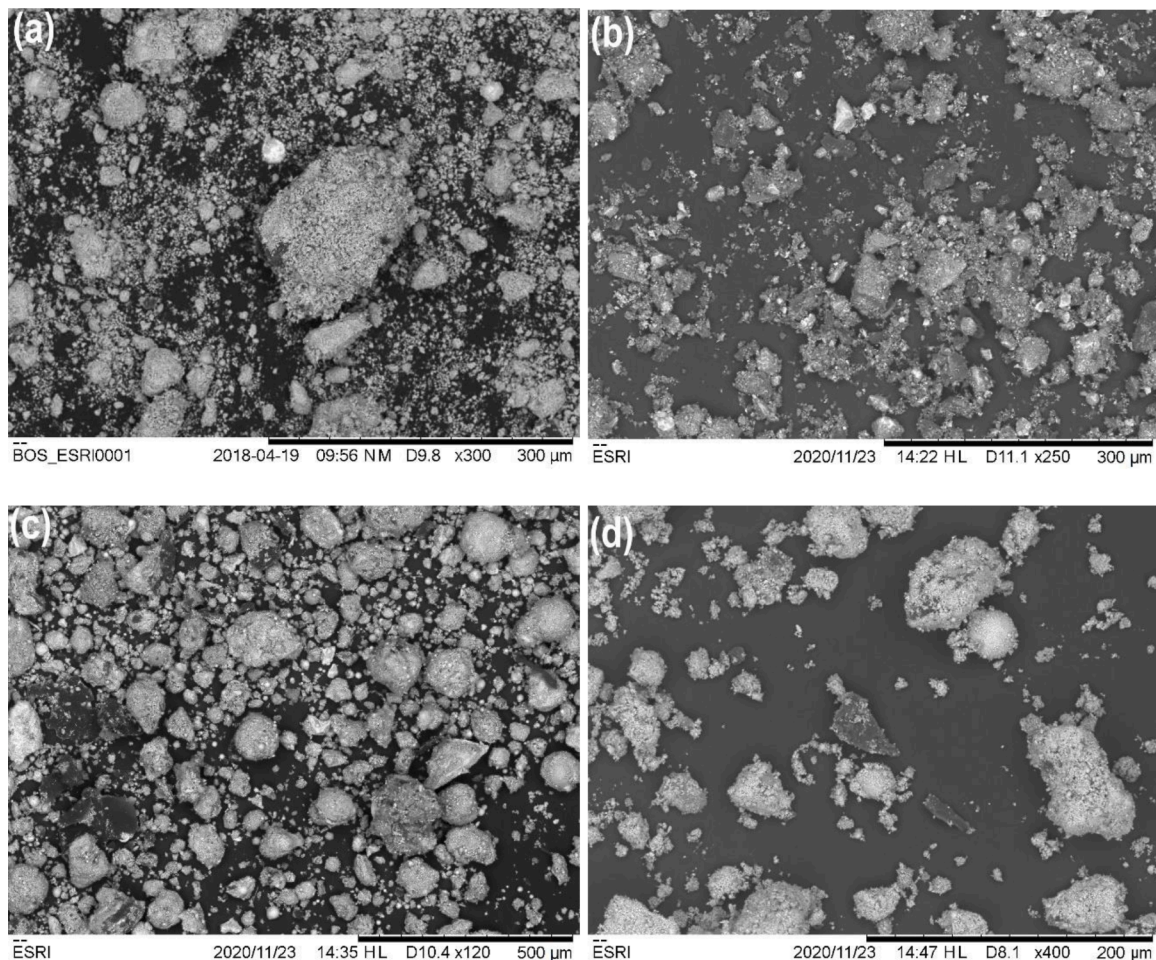


**Fig. 8.** SEM analysis of BOS Dust A (a), BF Dust A (b), BOS Dust B (c) and BOS Dust C (d).

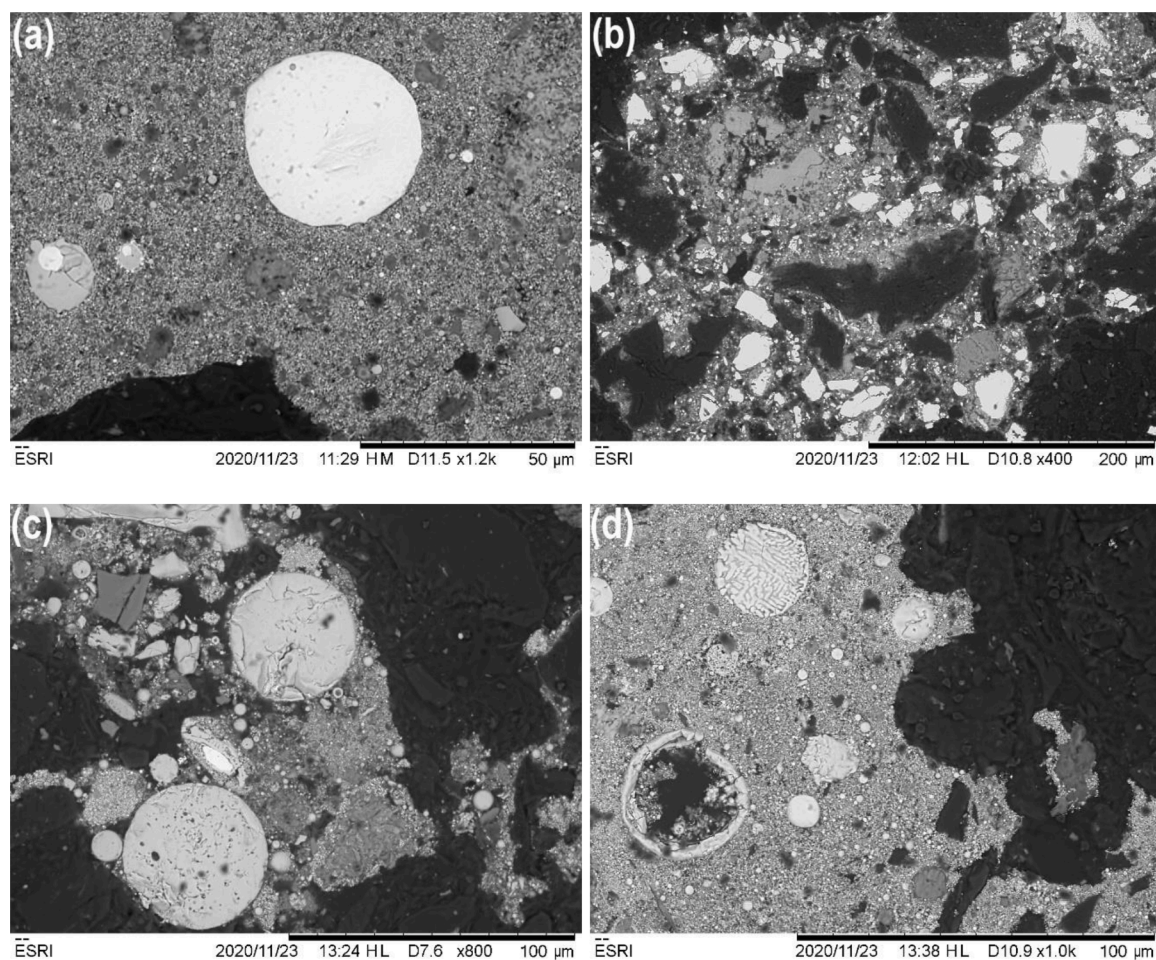


Fig. 9. Cross sectional analysis of BOS Dust A (a), BF Dust A (b), BOS Dust B (c) and BOS Dust C (d).

Table 7

Combustion analysis results for BOS Dust A, BF Dust A, BOS Dust B and BOS Dust C.

Material	Composition (wt.%)		
	C	S	C <sub>carbonate</sub>
BOS Dust A	3.95	<0.001	2.18
BF Dust A	40.49	0.62	0.71
BOS Dust B	6.74	0.005	0.75
BOS Dust C	9.69	0.014	0.75

formation mechanism primarily consisting of abrasion, whereas the spheroidal particles present in all three BOS dust samples they share a similar, fluid ejection-based formation mechanism.

### 3.6. Combustion analysis

Table 7 shows the results of combustion analysis for the four materials. As expected, the BOS steelmaking dust samples contain little carbon relative to BF Dust A. Fixed carbon is difficult to approximate for revert materials such as these, proximate analysis such as those performed thermogravimetrically for coals are inappropriate due to the reducible metals content of the material. An approximation of carbon in the form of carbonate is given in Table 7 based on the carbonate decomposition loss at around 700 °C observed during TGA-DSC experiments.

The results indicate that the majority of carbon present in BF Dust A is available for reduction as expected. What was less expected however is that all three BOS dust samples showed significant carbon content that

is not associated to carbonates and therefore may be useful as a reductant. It is unclear whether this carbon was introduced to the material as it was produced or whether it is the result of contamination and mixing during the stockpiling of the material.

Sulfur levels were expectedly low in samples produced during steelmaking, since hot metal has usually been desulfurized prior to charging into the BOS vessel. The level of sulfur in BF dust A was substantially higher, likely from the abraded coke and coal particles present in the material.

### 3.7. Mössbauer spectroscopy

<sup>57</sup>Fe Mössbauer spectroscopy was used to investigate the chemical environment of Fe species within the material. Samples were shown to be extremely chemically complex, with iron nuclei in multiple oxidation states and environments. While it was not possible to assign all sites used in the data fitting with the appropriate level of confidence, important structural information can be gleaned and compared to observations in XRD analysis through spectral fitting.

Previous work in the literature suggested that <sup>57</sup>Fe Mössbauer spectroscopy can be utilized to detect and differentiate the small amounts of ZnFe<sub>2</sub>O<sub>4</sub> that can be found in steelmaking dusts from spinel more easily than using powder XRD (Jabłońska et al., 2021; Vereš et al., 2010).

Detailed fitting information is provided in supplementary information tables S1-S4. Fitting of the data for the BOS Dust A shows a few easily assigned features (Fig. 10). The sextet fitted with zero quadrupolar splitting and chemical shift likely corresponds to metallic α-Fe

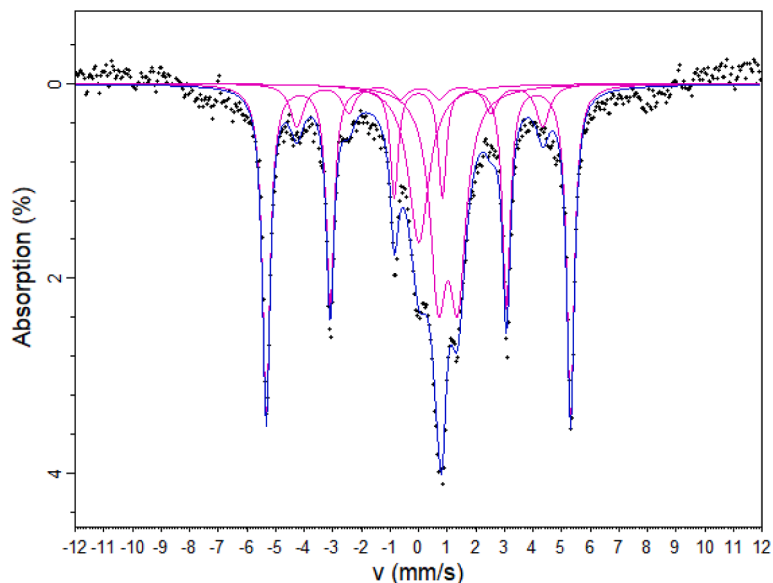


Fig. 10. Room temperature  $^{57}\text{Fe}$  Mössbauer spectroscopy data and associated fitting pattern for BOS Dust A. CS relative to  $\alpha\text{-Fe}$ .

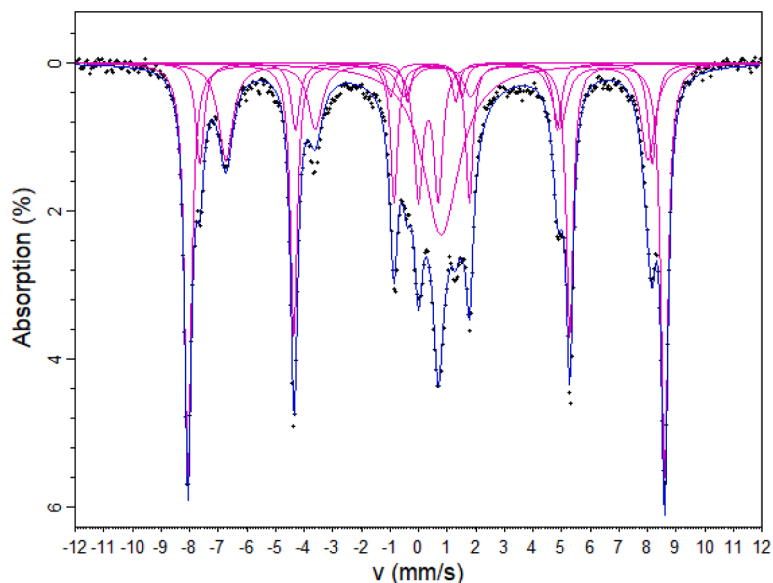


Fig. 11. Room temperature  $^{57}\text{Fe}$  Mössbauer spectroscopy data and associated fitting pattern for BF Dust A. CS relative to  $\alpha\text{-Fe}$ .

(CS = 0 mm/s,  $H = 33.0$  T) (Stevens et al., 2005) and the doublet (CS = 1.04 mm/s, QS = 0.67 mm/s) likely corresponds to  $\text{Fe}^{2+}$  in Wüstite (FeO) (Jabłońska et al., 2021). This is consistent with powder XRD analysis which also indicated the presence of metallic Fe and FeO.

For BF Dust A (Fig. 11), a sextet (CS = 0.37 mm/s,  $H = 51.6$  T) suggests the presence of hematite ( $\alpha\text{-Fe}_2\text{O}_3$ ) (Oh et al., 1998), while a second sextet (CS = 0.66 mm/s,  $H = 45.8$  T) indicates the presence of magnetite ( $\text{Fe}_3\text{O}_4$ ) (Stevens et al., 2005). Again, this is consistent with powder XRD and metallic iron analysis which suggests that BF Dust A was substantially more oxidized than the BOS dust samples.

BOS Dust B (Fig. 12) shows an exceptionally complicated spectral fit, due to the mineralogical complexity of the material. A sextet (CS = 0 mm/s,  $H = 33$  T) corresponds with metallic Fe as expected from the powder XRD pattern of the material, likewise a sextet (CS = 0.38 mm/s,  $H = 51.5$  T) likely corresponds to hematite ( $\alpha\text{-Fe}_2\text{O}_3$ ). A doublet (CS = 0.99 mm/s, QS = 0.69) suggests the presence of FeO.

BOS Dust C (Fig. 13) also shows complexity in the fitting of the data. Sextets correspond to hematite  $\alpha\text{-Fe}_2\text{O}_3$  (CS = 0.37 mm/s,  $H = 51.5$  T),

magnetite  $\text{Fe}_3\text{O}_4$  (CS = 0.3 mm/s, 48.8 T; CS = 0.60 mm/s,  $H = 45.0$  T), and metallic iron (CS = 0 mm/s,  $H = 33$  T) while a doublet (CS = 1.03 mm/s, QS = 0.65 mm/s) suggest the presence of FeO.

It is worth noting that franklinite ( $\text{ZnFe}_2\text{O}_4$ ) was not detected in any of the four samples via  $^{57}\text{Fe}$  Mössbauer spectroscopic analysis. It is possible that a small amount of sub-stoichiometric franklinite is present in the samples and is masked by overlapping signals around the region a characteristic hyperfine paramagnetic doublet would be expected (CS = 0.31 mm/s, QS = 0.70 mm/s) (Jabłońska et al., 2021), but based on the analyses performed in this work this was not possible to confirm.

Overall, the results from the  $^{57}\text{Fe}$  Mössbauer spectroscopy are consistent with powder XRD analyses but unlike in analysis undertaken by Vereš et al., zinc ferrite was not detected in the samples of BOS dust. This may be related to the design and operational differences between the plants in the UK where the samples for this study were taken and the plant in Košice, Slovakia where Vereš et al. obtained samples (Vereš et al., 2015).

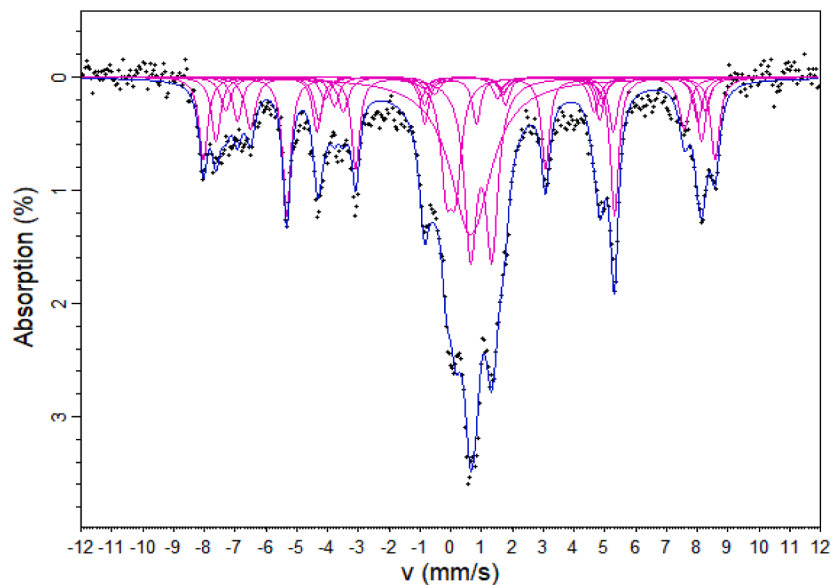


Fig. 12. Room temperature  $^{57}\text{Fe}$  Mössbauer spectroscopy data and associated fitting pattern for BOS Dust B. CS relative to  $\alpha\text{-Fe}$ .

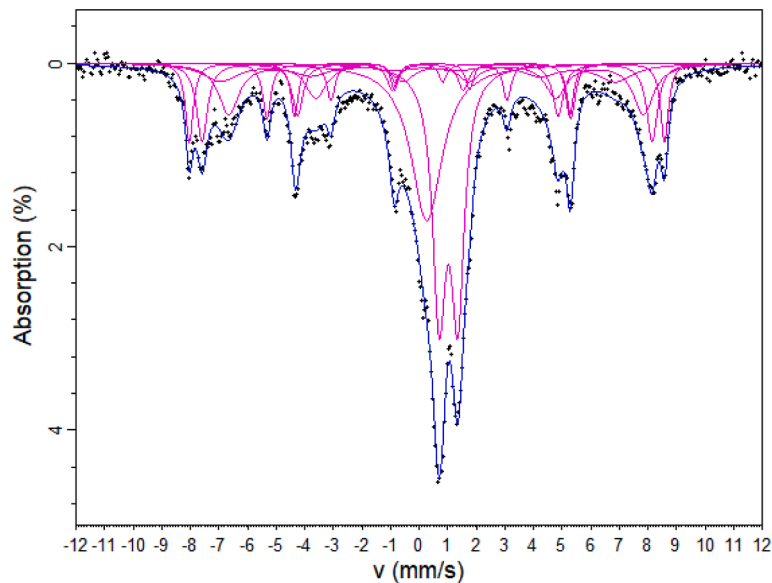


Fig. 13. Room temperature  $^{57}\text{Fe}$  Mössbauer spectroscopy data and associated fitting pattern for BOS Dust C. CS relative to  $\alpha\text{-Fe}$ .

#### 4. Conclusions

Analysis of samples of BOS Dust and BF Dust samples from UK plants has made clear that the materials are not suitable for direct recycling into the steelmaking process in their current condition. The BOS dust samples are highly metallized and contain significant amounts of Fe meaning that they have a high potential value for the steel recycler, but the levels of zinc in all three BOS dust samples and the BF dust sample were found to be too high for conventional recycling through the BF.

Crystallographic analysis via XRD diffraction suggested the BOS Dust B and BOS Dust C samples may contain a small amount of sub-stoichiometric zinc ferrite.  $^{57}\text{Fe}$  Mössbauer spectroscopic analysis was unable to differentiate any franklinite spinel from the complicated mineralogy of the samples if it is indeed present. The observation that the BOS Dust B and BOS Dust C materials may contain some zinc in the spinel form means hydrometallurgical processing may present process challenges such as lower zinc removal rates than expected.

These materials would be a prime candidate for recovery through

pyrometallurgical processing that is not sensitive to volatile metal loading, such as a rotary hearth furnace. Pyrometallurgical processing has the primary advantage that it is much less sensitive to variation in zinc mineralogy in the feedstock material than hydrometallurgical processing (Sammut et al., 2008). They are highly metallized meaning reductant use and subsequent  $\text{CO}_2$  emission is minimized. A furnace process such as FASTMET (McClelland and Metius, 2003), DRYIron (Ichikawa and Morishige, 2002) or INMETCO (Hanewald et al., 1992) would be suitable for recovery of the ferrous material as metallized direct reduced iron (DRI).

BF Dust A could be utilized as a supplementary reductant in a rotary hearth furnace to displace coal to reduce the environmental impact of the process. Processing of BOS dust with BF dust is not a new concept; McClelland et al. reported on the chemistry of typical input and output material to Kobe Steel's Kakogawa FASTMET plant (McClelland and Metius, 2003). The study estimated that FASTMET production costs for DRI with chemical composition as shown in Table 8, from BF dust, EAF dust and BOS dust was between \$150 - \$200 per tonne of DRI, and the

Table 8

Raw material and produced direct reduced iron chemical composition for the commercial Kakogawa FASTMET plant.

Material	Composition (wt.%)								
	Fe <sub>Tot</sub>	Fe <sub>Met</sub>	C	S	SiO <sub>2</sub>	Al <sub>2</sub> O <sub>3</sub>	CaO	MgO	Zn
Kakogawa BF Dust	31.8	–	37.6	0.70	4.10	–	3.1	–	1.2
Kakogawa BOS dust	53.6	–	0.70	0.17	6.18	0.315	5.0	0.185	2.54
Kakogawa FASTMET DRI	68.0	57.8	2.00	0.52	5.95	–	4.35	–	–

similarities between the raw materials used are clear.

The major disadvantage of the use of BF dust as a reductant is inclusion of sulfur into the metallized product. The produced DRI is metallized enough to be directly integrated as a scrap substitute into a basic oxygen steelmaking vessel but the high levels of sulfur in the material would limit its use and value. Instead, so-called revert DRI (DRI produced from recycled steelmaking by-product materials) is usually recycled to a blast furnace, which is less sensitive to high sulfur loading but with a lower cost benefit than recycling to the BOS vessel (Vicente et al., 2020).

The United Kingdom would be an excellent candidate for a large scale pyrometallurgical processing plant for zinc bearing wastes due to the suitability of material for integration into the process, the relative ease of material acquisition due to the countries geographic size as well as the fact that steel producing sites typically have excellent rail and sea freight infrastructure for movement of material to a centralized processing site.

#### Declaration of Competing Interest

One of the authors (D.T.) is employed by Tata Steel Strip Products UK who have supplied two of the samples and required that samples be anonymized. The remaining authors declare that they have no competing financial interests or personal relationships that could have appeared to influence the work reported in this paper.

#### Acknowledgements

Financial support was provided by Materials and Manufacturing Academy (M2A) that has been made possible through funding from the European Social Fund via the Welsh Government, Swansea University EPSRC impact acceleration account, the COATED doctoral training center, the European Regional Development Fund (ERDF) and SMART Expertise Wales for funding Materials Advanced characterisation center (MACH1) and Combinatorial Metallurgy (COMET) project at Swansea University, and Tata Steel UK. Additional support is provided by the Reducing Industrial Carbon Emissions (RICE) operations funded by the Welsh European Funding Office (WEFO) through the Welsh Government. The authors would like to specifically acknowledge the BOS lab team at Tata Steel Port Talbot for assistance with XRF analysis.

#### Supplementary materials

Supplementary material associated with this article can be found, in the online version, at doi:10.1016/j.rcradv.2022.200073.

#### References

Al-Anazi, A., Abdelraheem, W.H., Scheckel, K., Nadagouda, M.N., O'Shea, K., Dionysiou, D.D., 2020. Novel franklinite-like synthetic zinc-ferrite redox nanomaterial: synthesis, and evaluation for degradation of diclofenac in water. *Appl. Catal. B Environ.* 275 <https://doi.org/10.1016/j.apcatb.2020.119098>.

Bagatini, M.C., Zymła, V., Osório, E., Cezar, A., Vilela, F., 2011. Characterization and reduction behavior of mill scale. *ISIJ Int.* 51, 1072–1079. <https://doi.org/10.2355/isijinternational.51.1072>.

Besta, P., Janovská, K., Samolejová, A., Beránková, A., Vozňáková, I., Hendrych, M., 2013. The cycle and effect of zinc in the blast-furnace process. *Metalurgija* 52, 197–200.

British Steel, n.d. The history of British steel [WWW Document]. URL <https://britishsteel.co.uk/media/323481/history-of-british-steel.pdf> (accessed 6.11.20). 2020.

Cantarino, M.V., De Carvalho Filho, C., Borges Mansur, M., 2012. Selective removal of zinc from basic oxygen furnace sludges. *Hydrometallurgy* (111–112.), 124–128. <https://doi.org/10.1016/j.hydromet.2011.11.004>.

Chatterjee, A., 2012. Sponge iron production by direct reduction of iron oxide, Second. ed.

d-maps, 2020. Map of the United Kingdom [WWW Document]. URL [https://d-maps.com/pays.php?num\\_pay=218&lang=en](https://d-maps.com/pays.php?num_pay=218&lang=en).

Dankwah, J.R., Amoah, T., Dankwah, J., Fosu, A.Y., 2015. Recycling mixed plastics waste as reductant in ironmaking. *Ghana Min. J.* 15, 73–80.

Donald, J., Pickles, C., 1996. A kinetic study of the reaction of zinc oxide with iron powder. *Pyrometallurgy* 27, 363–374. <https://doi.org/10.1007/BF02914899>.

Donald, J., Pickles, C., 1996. Reduction of electric arc furnace dust with solid iron powder. *Can. Metall. Q.* [https://doi.org/10.1016/0008-4433\(96\)00009-2](https://doi.org/10.1016/0008-4433(96)00009-2).

Report, E.N.D.S., 1992. Scottish steel works leaves massive clean-up bill. *ENDS Rep.* URL <https://www.endsreport.com/article/1577364/scottish-steel-works-leaves-massive-clean-up-bill>.

Hahn, I., Neuschütz, D., 2002. Ejection of steel and slag droplets from gas stirred steel melts. *Ironmak. Steelmak.* 29, 219–223. <https://doi.org/10.1179/030192302225004115>.

Halt, J.A., Nitz, M.C., Kawatra, S.K., Dube, M., 2015. Iron ore pellet dustiness part i : factors affecting dust generation. *Miner. Process. Extr. Metall. Rev.* 36, 258–266. <https://doi.org/10.1080/08827508.2014.928876>.

Hanewald, R.H., Munson, W.A., Schweyer, D.L., 1992. Processing steel wastes pyrometallurgically at INMETCO. *Mining. Metall. Explor.* 9, 169–173. <https://doi.org/10.1002/9781118788073.ch34>.

HM Revenue & Customs, 2020. Excise Notice LFT1 [WWW Document]. URL <https://www.gov.uk/government/publications/excise-notice-lft1-a-general-guide-to-landfill-tax/excise-notice-lft1-a-general-guide-to-landfill-tax#mining-and-quarrying-material> (accessed 4.1.20).

Holappa, L.E., Kekkonen, M., 2000. Comparison of Different Coal Based Direct Reduction Processes. *Univ. of Technology, ISBN, Helsinki*, 951-22-5134-5.

Ichikawa, H., Morishige, H., 2002. Effective use of steelmaking dust and sludge by use of rotary hearth furnace. *Nippon Steel Tech. Rep.* 86, 35–38.

Jaafar, I., 2014. Chlorination For the Removal of Zinc from Basic Oxygen Steelmaking (bos) By-Product. PhD Thesis, Cardiff University.

Jabłońska, M., Rachwał, M., Wawer, M., Kądziołka-Gawel, M., Teper, E., Krzykowski, T., Smolka-Danielowska, D., 2021. Mineralogical and chemical specificity of dusts originating from iron and non-ferrous metallurgy in the light of their magnetic susceptibility. *Minerals* 11, 1–20. <https://doi.org/10.3390/min11020216>.

Kelebek, S., Yörük, S., Davis, B., 2004. Characterization of basic oxygen furnace dust and zinc removal by acid leaching. *Miner. Eng.* 17, 285–291. <https://doi.org/10.1016/j.mineng.2003.10.030>.

Klut, P., Tesselar, E., Barel, J., Engel, E., Corus, D., 2016. Blast furnace zinc control, *Millennium Steel* 46–52, 2016.

Kmita, A., Żukrowski, J., Kuciakowski, J., Marciszko-Wiąckowska, M., Żywczak, A., Lachowicz, D., Gajewska, M., Sikora, M., 2021. Effect of thermal treatment at inert atmosphere on structural and magnetic properties of non-stoichiometric zinc ferrite nanoparticles. *Metall. Mater. Trans. A Phys. Metall. Mater. Sci.* 52, 1632–1648. <https://doi.org/10.1007/s11661-021-06154-3>.

Kuwauchi, Y., 2012. A mathematical model for carbothermic reduction of dust-carbon composite agglomerates. *ISIJ Int.* 53, 1097–1105. <https://doi.org/10.2355/isijinternational.53.1097>.

Liu, S., Loper, C.R., 1991. The formation of kish graphite. *Carbon N Y* 29, 547–555. [https://doi.org/10.1016/0008-6223\(91\)90119-4](https://doi.org/10.1016/0008-6223(91)90119-4).

Lysenko, E.N., Surzhikov, A.P., Zhuravkov, S.P., Vlasov, V.A., Pustovalov, A.V., Yavorovsky, N.A., 2014. The oxidation kinetics study of ultrafine iron powders by thermogravimetric analysis. *J. Therm. Anal. Calorim.* 115, 1447–1452. <https://doi.org/10.1007/s10973-013-3456-x>.

MacKillop, F., 2009. The construction of “waste” in the UK steel industry. *J. Environ. Plan. Manag.* 52, 177–194. <https://doi.org/10.1080/09640560802666529>.

Manoj, B., 2016. A comprehensive analysis of various structural parameters of Indian coals with the aid of advanced analytical tools. *Int. J. Coal Sci. Technol.* 3, 123–132. <https://doi.org/10.1007/s40789-016-0134-1>.

McClelland, J.M., Metius, G.E., 2003. Recycling ferrous and nonferrous waste streams with FASTMET. *JOM* 55, 30–34. <https://doi.org/10.1007/s11837-003-0101-3>.

Meraikib, M., 1995. Activity of silica in the slag of an electric arc furnace using direct reduced iron for steelmaking. *ISIJ Int.* 35 (7), 845–850. <https://doi.org/10.2355/isijinternational.35.845>.

Mikhail, S.A., Turcotte, A.-M., 1998. Thermal reduction of steel-making secondary materials. *Thermochim. Acta* 311, 113–119. [https://doi.org/10.1016/S0040-6031\(97\)00430-9](https://doi.org/10.1016/S0040-6031(97)00430-9).

Mombelli, D., Di Cecca, C., Mapelli, C., Barella, S., Bondi, E., 2016. Experimental analysis on the use of BF-sludge for the reduction of BOF-powders to direct reduced iron (DRI) production. *Process Saf. Environ. Prot.* 102, 410–420. <https://doi.org/10.1016/j.psep.2016.04.017>.

- Narita, C.Y., Mourao, M.B., Takano, C., 2015. Development of composite briquettes of iron ore and coal hardened by heat treatment. *Ironmak. Steelmak.* 42, 548–552. <https://doi.org/10.1179/1743281214Y.0000000260>.
- Nyridena, R.L., 1991. The processing of steelmaking flue-dust: a review. *Miner. Eng.* 4, 1003–1025. [https://doi.org/10.1016/0892-6875\(91\)90080-F](https://doi.org/10.1016/0892-6875(91)90080-F).
- Oh, J., Cook, D., Townsend, H., 1998. Characterization of iron oxide commonly formed as corrosion products on steel. *Hyperfine Interact.* <https://doi.org/10.1023/a:1011076308501>.
- Onoye, T., Satoh, Y., Manabu, T., Kamatani, K.S., 1981. Effects of alkalis and zinc on the wear of the blast furnace refractories and the tuyere displacement. *Trans. ISIJ* 21, 839–845. <https://doi.org/10.2355/isijinternational1966.21.839>.
- Pickles, C.A., 2008. Thermodynamic analysis of the separation of zinc and lead from electric arc furnace dust by selective reduction with metallic iron. *Sep. Purif. Technol.* 59, 115–128. <https://doi.org/10.1016/j.seppur.2007.05.032>.
- Rancourt, D., 1998. Recoil Mössbauer spectral analysis software.
- Ray, S.K., Chattopadhyay, G., Ray, A.K., 1997. Evaluation of dust generated from basic oxygen furnace steel making. *J. Air Waste Manag. Assoc.* 47, 716–721. <https://doi.org/10.1080/10473289.1997.10463929>.
- Rhodes, C., Hutton, G., 2018. UK Steel industry : Statistics and Policy. House of Commons, Library.
- Ruíz-Baltazar, A., Esparza, R., Rosas, G., Pérez, R., 2015. Effect of the surfactant on the growth and oxidation of iron nanoparticles. *J. Nanomater.* 2015, 240948 <https://doi.org/10.1155/2015/240948>.
- Salama, W., El Aref, M., Gaupp, R., 2015. Spectroscopic characterization of iron ores formed in different geological environments using FTIR, XPS, Mössbauer spectroscopy and thermoanalyses. *Spectrochim. Acta - Part A Mol. Biomol. Spectrosc.* 136, 1816–1826. <https://doi.org/10.1016/j.saa.2014.10.090>.
- Sammut, M.L., Rose, J., Masion, A., Fiani, E., Depoux, M., Ziebel, A., Hazemann, J.L., Proux, O., Borschneck, D., Noack, Y., 2008. Determination of zinc speciation in basic oxygen furnace flying dust by chemical extractions and X-ray spectroscopy. *Chemosphere.* <https://doi.org/10.1016/j.chemosphere.2007.09.063>.
- Souza, F.De, Braganc, S.R., 2013. Thermogravimetric analysis of limestones with different contents of MgO and microstructural characterization in oxy-combustion. *Thermochim. Acta* 561, 19–25. <https://doi.org/10.1016/j.tca.2013.03.006>.
- Steer, J., Grainger, C., Griffiths, A., Griffiths, M., Heinrich, T., Hopkins, a., 2014. Characterisation of BOS steelmaking dust and techniques for reducing zinc contamination. *Ironmak. Steelmak.* <https://doi.org/10.1179/1743281213Y.0000000106>.
- Stevens, J.G., Khasanov, A.M., Miller, J.W., Pollak, H., Li, Z., 2005. *Mössbauer Mineral Handbook*. Effect Data Center, Mössbauer.
- Stewart, D.J.C., Barron, A.R., 2020. Pyrometallurgical removal of zinc from basic oxygen steelmaking dust – a review of best available technology. *Resour. Conserv. Recycl.* 157, 104746 <https://doi.org/10.1016/j.resconrec.2020.104746>.
- Trinkel, V., Mallow, O., Aschenbrenner, P., Rechberger, H., Fellner, J., 2016. Characterization of blast furnace sludge with respect to heavy metal distribution. *Ind. Eng. Chem. Res.* 55, 5590–5597. <https://doi.org/10.1021/acs.iecr.6b00617>.
- Trung, Z.H., Kukurugya, F., Takacova, Z., Orac, D., Laubertova, M., Miskufova, A., Havlik, T., 2011. Acidic leaching both of zinc and iron from basic oxygen furnace sludge. *J. Hazard. Mater.* 192, 1100–1107. <https://doi.org/10.1016/j.jhazmat.2011.06.016>.
- Veres, J., Sepelák, V., Hredzák, S., 2015. Chemical, mineralogical and morphological characterisation of basic oxygen furnace dust. *Miner. Process. Extr. Metall.* 124, 1–8. <https://doi.org/10.1179/1743285514Y.0000000069>.
- Veres, J., Jakabský, S., Sepelák, V., 2010. Chemical, physical, morphological and structural characterization of blast furnace sludge. *Diffus. Fundam.* 12, 88–91.
- Vicente, A., Picon, A., Barco, E., 2020. New method for estimating the economic penalties of ferrous scraps in the steelmaking industry due to material degradation during its storage in scrap yards. *Ironmak. Steelmak.* 47, 473–481. <https://doi.org/10.1080/03019233.2020.1748433>.
- World Steel Association, 2018. World steel association fact sheet. *Steel Industry By-Products*.
- Xu, Z., Hwang, J., Greenlund, R., Huang, X., Luo, J., Anschuetz, S., 2003. Quantitative determination of metallic iron content in steel-making slag. *J. Miner. Mater. Charact. Eng.* 02, 65–70. <https://doi.org/10.4236/jmmce.2003.21006>.
- Yang, Yang, Liu, X., Yang, Yong, Xiao, W., Li, Z., Xue, D., Li, F., Ding, J., 2013. Synthesis of nonstoichiometric zinc ferrite nanoparticles with extraordinary room temperature magnetism and their diverse applications. *J. Mater. Chem. C* 1, 2875–2885. <https://doi.org/10.1039/c3tc00790a>.
- Yuan, P., Shen, B., Duan, D., Adwek, G., Mei, X., Lu, F., 2017. Study on the formation of direct reduced iron by using biomass as reductants of carbon containing pellets in RHF process. *Energy* 141, 472–482. <https://doi.org/10.1016/j.energy.2017.09.058>.
- Zhang, W., Tian, Y., Liu, D.-C., Wang, F., Yang, B., Xu, B.-Q., 2020. Experimental study on the thermal volatilization and condensation of zinc at 10 Pa and 200 Pa. *J Mater Res Technol* 9, 3590–3597. <https://doi.org/10.1016/j.jmrt.2020.01.097>.
- Zhang, Y., Xu, X., 2020. Machine learning lattice constants for spinel compounds. *Chem. Phys. Lett.* <https://doi.org/10.1016/j.cplett.2020.137993>.